

Mariusz KASTEK¹, Tadeusz PIĄTKOWSKI¹, Martin CHAMBERLAND², Philippe LAGUEUX²¹ INSTYTUT OPTOELEKTRONIKI, WOJSKOWA AKADEMIA TECHNICZNA, ul. gen. S. Kaliskiego 2, 00-908 Warszawa² TELOPS INC., 100-2600 St-Jean-Baptiste, Québec, Qc, G2E 6J5, Canada**Method and software for hyperspectral data analysis focused on automatic detection and identification of chemical agents****Ph.D. Mariusz KASTEK**

He received M.Sc. and Ph.D. degree in electronics specialization optoelectronics from Military University of Technology (MUT). He works on many projects supporting by Polish Ministry of Science focus on developing infrared cameras. He works on developing new algorithms analysis of multispectral and hyperspectral data for detection objects in short and long infrared. Presently he is working as an assistant professor in Department of Infrared Technology and Thermovision at Institute of Optoelectronics MUT.



e-mail: mkastek@wat.edu.pl

Ph.D. Tadeusz PIĄTKOWSKI

Tadeusz Piątkowski, is an assistant professor in the Institute of Optoelectronics at Military University of Technology (MUT). He received a M.Sc. degree in optical science and M.Sc. degree in electronics from the Warsaw University of Technology in 1981 and 2002 respectively, Ph.D. degree in optoelectronics from MUT in 2004. He currently works for the MUT as a member of the Infrared Technology and Thermovision Section. His research interests include infrared imaging, hyperspectral imaging, and signal processing.



e-mail: tpiatkowski@wat.edu.pl

Ph.D. Martin CHAMBERLAND

Martin Chamberland graduated in Electrical Engineering (Ph.D. 1995) from Université Laval (Quebec City). Martin is a worldwide recognized expert in the area of imaging Fourier Transform Spectrometers (iFTS). He acted as lead systems engineer at Bomem (1994-2000) prior to founding Telops in 2000. Martin is currently the VP Technology at Telops and he is responsible for new products and applications development.



e-mail: martin.chamberland@telops.com

M.Sc. Philippe LAGUEUX

Philippe Lagueux graduated in Physics Engineering (B.Sc. - 1999) and Physics (M.Sc. - 2002) from Université Laval (Quebec City). Philippe joined Telops in 2000 as leading optical systems engineer and largely contributed to the development of the Telops Infrared sensor heritage and commercial product portfolio. Philippe is currently manager for business development while securing support to technical sales.



e-mail: philippe.lagueux@telops.com

Abstract

This paper presents detection and identification of gases using an infrared imaging Fourier-transform spectrometer. The principle of operation of the spectrometer and the method for gases detection and identification is shown in the paper. The new software with implementation of method based on Clutter Match Filter, focused on detection and identification of gases is presented. Some results of the detection of various types of gases are also given.

Keywords: hyperspectral detection, infrared imaging spectroradiometer.

Metoda i oprogramowanie do analizy hyperspektralnych danych przeznaczona do automatycznego wykrycia i identyfikacji skażeń chemicznych

Streszczenie

Wykrywanie zagrożeń we współczesnym świecie jest jednym z głównych zadań stawianych przed urządzeniami optoelektronicznymi. Skażenia chemiczne to jedne z wielu zagrożeń które są wykrywane za pomocą obserwacyjnych urządzeń podczerwieni. Jednym z zaawansowanych technologicznie urządzeń jest fourierowski spektrometr obrazowy wyposażony w matrycę 320x256 detektorów typu MCT (Mercury Cadmium Telluride). Konstrukcja spektrometru oparta na układzie interferometru Michelsona-Moreya umożliwia uzyskanie rozdzielczości spektralnej od 0.25 cm⁻¹ do 150 cm⁻¹ w zakresie od 830 cm⁻¹ (12 μm) do 1290 cm⁻¹ (7.75 μm) z częstotliwości rejestracji obrazów 0.2 Hz. Zasada działania spektrometru oraz jego parametry techniczne zostały przedstawione w pierwszej części artykułu natomiast dalsza część poświęcona jest metodzie analizy hyperspektralnych danych rejestrowanych za jego pomocą. Analiza danych oparta na dwóch zaawansowanych metodach filtracji bazujących na CMF (Clutter Match Filter) oraz bazie danych charakterystyk widmowych gazów umożliwia na automatyczną detekcję i identyfikację wybranych związków chemicznych. Metoda została przetestowana podczas badań laboratoryjnych, a pozytywne wyniki pozwoliły na implementację jej do komercyjnego oprogramowania. Uzyskane wyniki podczas testów przeprowadzonych w warunkach rzeczywistych (szczególnie podczas detekcji i identyfikacji związków chemicznych podczas swobodnego parowania) świadczą o dużej skuteczności opracowanej metody.

Keywords: hyperspektralna detekcja, obrazowy spektrometr podczerwieni.

1. Introduction

A problem of remote detection of chemical substances appears in many, sometimes extremely different, fields of human activities. Applications of detection devices include monitoring of technological processes, diagnostics of industrial installations, monitoring of natural environment, and military purposes. Such diversity has caused development of many detection methods employing various physical phenomena due to which detection and identification of chemical compounds are possible.

The devices operating in infrared, used for detection of chemical substances (gases) in the atmosphere have spectral characteristics and resolution matched to the absorption bands of compounds to be detected. Two types of such devices can be distinguished. One is a system similar to the typical thermal camera but additionally equipped with a filter system ensuring the required spectral resolution and the signal analysis system. The other type includes a device based on the principles of Fourier spectroscopy (Fourier Transform Infrared Spectroscopy - FTIR) that is expensive and so not readily available.

Fourier-transform spectrometers are renowned instruments, particularly well-suited to remotely provide excellent estimates of quantitative data. Many authors have presented how they use the conventional (non-imaging) FTS to perform quantification of distant gas emissions. Amongst others, we should mention the important contributions made by Harig [1]. Other groups have developed similar approaches, however limiting their study to optically thin plumes [2], to dedicated instruments performing optical subtraction [3], or introducing Bayesian algorithms to maximize the use of a priori information. On the other hand, detection and quantification activities with an imaging Fourier-transform spectrometer (iFTS) have been first presented by Spisz [4].

The present paper deals with the remote gas detection and identification from turbulent stack plumes with an iFTS. First, it presents the modeling that is required in order to get an appropriate understanding of both the scene and the instrument.

Finally, the results are presented to demonstrate the capabilities and the performance of the remote gas detection and identification by using hyperspectral data obtained from the Telops HyperCam and the new software. The latter is described in detail in prior references [3, 5, 6].

2. Imaging Fourier Transform Spectroradiometer

The infrared imaging Fourier-transform spectrometer (IFTS) – Hyper-Cam LWIR – used for experiments was built by Telops Inc.. This IFTS uses 320x256 pixel Mercury Cadmium Telluride (MCT) focal plane arrays (FPA) with a 6° x 5° FOV. The FPA has a Stirling cooler to provide good noise figures in a field ready package. Spectral information is obtained using a technique called Fourier Transform Infrared Radiometry (FTIR). FTIR is a classical interference based technique applied to gas spectroscopy that uses a Michelson interferometer to mix an incoming signal with itself at several different discrete time delays. The resulting time domain waveform, called an interferogram, is related to the power spectrum of the scene through the Fourier transform. An interferogram for each pixel in an image is created by imaging the output of the interferometer onto a focal plane array and collecting data at each discrete time delay. Advantages of using the FTIR sensor over a filter or grating based system include higher resolution for equal cost and the absence of misalignment of different color images due to platform motion. However, FTIR does have the disadvantage of producing a slower frame rate than filter based systems because twice as many points are taken for the same number of spectral points. For atmospheric tracking of gases however, the LWIR sensor has the sufficient frame rate [6].

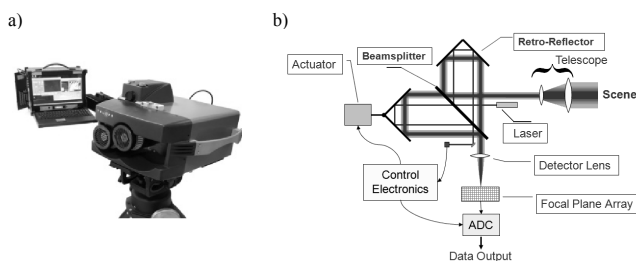


Fig. 1. The infrared imaging Fourier-transform spectrometer (IFTS) HyperCam (a) and the block diagram of the imaging Fourier-transform spectroradiometer (b)
Rys. 1. Obrazowy fourierowski spektrometr HyperCam podczas pomiarów (a) i schemat blokowy obrazowego fourierowskiego spektrometru (b)

Data for this collection can be taken from 0.25 cm⁻¹ to 150 cm⁻¹ spectral resolution between 830 cm⁻¹ (12 μm) and 1290 cm⁻¹ (7.75 μm) at a frame rate of 0.2 Hz. In addition to the infrared data, visible imagery was taken using a camera that was boresighted to the IR sensor. Fig. 1a shows a picture of a HyperCam LWIR. The sensor is controlled by a field computer and the data is stored on a RAID drive to guarantee the data integrity [7].

The imaging Fourier-transform spectroradiometer – HyperCam – uses the layout of a Michelson interferometer. Its schematic diagram, showing the elements responsible for the change of the optical path length, is shown in Fig. 1b.

In the presented system there are used retro-reflectors instead of flat mirrors. As a result, it is easier to move a mirror keeping the reflecting plane in the constant position with respect to the optical axis. It should be mentioned here that the interferometer works in the far infrared range, thus the necessary difference in optical paths requires large mirror travel. For such long moves in a classical setup with flat mirrors the skew of the mirror plane is difficult to avoid, which may result in considerable measurement errors. The solution presented in Fig. 1b. minimizes such errors.

The main difference between the standard and imaging interferometer is the application of a focal plane array (FPA) of detector type. The imaging device can be described as the classical

interferometer multiplied by the number of pixels in the array. As a result, the spectral analysis of interferograms at single pixels gives the spectral information of the entire image. The analysis of incident radiation at pixel level is identical for every array element.

The change in amplitude is a result of optical path difference x (this is a double offset retro-reflectors), for λ_i wavelength. The detector response is proportional to the radiant intensity of incident radiation:

$$I(x) = I_i \cos^2\left(2\pi \frac{x}{\lambda_i}\right). \quad (1)$$

Considering the trigonometric relations for the cosine of double angle and limiting the analysis to the variable component only, the radiant intensity is the function of the optical path. For the sources with continuous radiation characteristics in the range from λ_1 to λ_2 , whose spectral characteristic is described by a function $S(\lambda)$, the radiant intensity can be described as:

$$I(x) = \int_{\lambda_1}^{\lambda_2} S(\lambda) \cos\left(4\pi \frac{x}{\lambda}\right) d\lambda. \quad (2)$$

The intensity is recorded for various offsets retro-reflectors from $-OPD_{max}$ to $+OPD_{max}$. Based on that data, spectral distribution for a given pixel detector can be recreated using the inverse Fourier transform, by calculating the integral:

$$S(\lambda) = \int_{-\infty}^{+\infty} I(x) \cos\left(2\pi \frac{x}{\lambda}\right) dx. \quad (3)$$

In practical applications the optical path difference is realized in the finite, symmetrical range $\pm d$, so the relation (3) assumes the following form:

$$S(\lambda) = \int_{-d}^{+d} I(x) \cos\left(2\pi \frac{x}{\lambda}\right) dx. \quad (4)$$

The spectral distribution for an entire image is obtained by performing the analysis according to (4) for every pixel of an FPA array. The results can be treated as 3-dimensional data (two image coordinates and a wavelength – datacube).

3. Method of detection and identification of chemical agents

The target detection and identification algorithm is generally based on three key factors: the composition of the analyzed pixel, the type of the model used to estimate the variability of the target and background spaces, and the model used to describe the pure and mixed pixels. The mathematical representation of a mixed pixel depends on whether the background (or target) space is estimated statistically or geometrically. The considered sub-pixel target detection algorithms are of a stochastic nature. When the background is entirely represented by its statistics, the detection problem consists in extracting the targeted spectral signatures from a background noise.

The CMF is a recognized method and provides a standard by which to compare other detection techniques in the vector-valued observation paradigm. Consider the vector-valued signal model:

$$r_t = z_t + e_t b. \quad (5)$$

where the pixels in an image are indexed by t and the background image information is z . The vectors r_t , z_t , b are $m \times 1$ column vectors. A signal of interest is denoted by b and a signal “strength” is denoted by e_t . In this situation it may be desired to detect the presence of b among the background information.

The clutter matched filter is an example of an optimal detector for an additive signal on a gaussian background in vector-valued data. The clutter matched filter is commonly written as

$$CMF_i = \frac{b^T K^{-1} r_i}{\sqrt{b^T K^{-1} b}} \quad (6)$$

There are several ways to arrive at this expression [8]. One method is to maximize a signal-to-clutter ratio much like the one maximized for Fisher's discriminant. The discriminant function described by Fisher [9] is the oldest classification technique used in this study. The goal of this discriminant is to project multi-class data ($x \in X_i, i \in \{0, 1, \dots, k\}$) with high dimensionality to a low (perhaps one) dimensionality, while maintaining the separation of the classes. This discriminant is developed here in the simplest two-class case, where it is desired to project the data x onto a single dimension (by some $y = w^T x$) in such a way that maximizes the separation of the two classes is maximized. The set of the projected data y could then be separated into two groups Y_1 and Y_2 that should correspond very closely to the original classes X_1 and X_2 . Maximizing the separation of these two classes in the lower dimension can be made in a meaningful way by maximizing the difference between class means relative to some description of the variance of the classes.

This method uses Lagrange multipliers to find the maximum of the signal-to-clutter ratio and the minimum of the constrained optimization cost function is found. Another common method is to assume the background data to be Gaussian and perform a hypothesis test on the presence of the signal b in the observation. This is the approach that will be taken here.

Let the observations have this probability density function:

$$f(r) = \frac{1}{(2\pi)^m / \sqrt{|K|}} \exp\left(-\frac{1}{2}(r-\mu)^T K^{-1}(r-\mu)\right) \quad (7)$$

where μ is the mean and K is the covariance. Propose a hypothesis test on the presence of signal in the observation. This really tests for a shift in the mean, as shown in the hypotheses below. Let

$$H_0 : \mu = \mu_z \quad (8)$$

$$H_1 : \mu = \mu_z + e b \quad (9)$$

and form the likelihood ratio for this test. This likelihood ratio (LR) can be written as

$$LR(r) = \frac{\exp\left(-\frac{1}{2}(r-\mu-e b)^T K^{-1}(r-\mu-e b)\right)}{\exp\left(-\frac{1}{2}(r-\mu)^T K^{-1}(r-\mu)\right)} \quad (10)$$

It is important to understand that there are many paths that photons can take to arrive at a sensor pointed at the ground. There are photons emitted by materials at their respective temperatures, and transmissions through gasses, as well as absorptions and reflections by opaque objects. Though there are many paths to consider, there are only a few that significantly contribute to the signal measured at the sensor in LWIR measurements. Only those important paths will be considered in this development, which is drawn mainly from the literature focusing on the detection problem, but also from some works done on artificial plume insertion [8-12]. Firstly, a model will be developed for paths that arrive at a sensor which is pointed at the ground, but not viewing any gaseous plumes in the atmosphere. The main contributing paths to the signal in this situation are atmospheric upwelling (L_u), background (ground) radiance (L_g), and noise (L_n). Atmospheric upwelling is radiance that comes from the atmosphere thermal

emission at its temperature. The ground radiance is described as a combination of the thermal emission of an object at the ground temperature scaled by the emissivity of the material emitting (ϵ_g), and atmospheric downwelling. The noise term encompasses a few effects including the noise on the focal plane and the thermal emission of the sensor itself onto its focal plane. The combination measured at the sensor can be stated as:

$$L_{clear}(\lambda) = L_u(\lambda) + L_g(\lambda)\tau_{atm}(\lambda) + L_n(\lambda) \quad (11)$$

which describes the attenuation of the ground radiance by the transmissivity of the atmosphere, τ_{atm} . This also denotes the wavelength (λ) dependence of all these terms. The background radiance must be further broken up into constituent terms:

$$L_g(\lambda) = B(\lambda, T_g)\epsilon_g(\lambda) + L_d(\lambda)(1 - \epsilon_g(\lambda)) \quad (12)$$

The background material is held to be at some temperature T_g , and it is assumed to be radiating as a perfect blackbody does. The $B(\lambda, T_g)$ function represents the Planck function for radiating blackbodies. This radiation is scaled by the emissivity of the material, ϵ_g . The other significant contribution to the background radiance term is the reflected atmospheric downwelling. The atmosphere, as previously mentioned, radiates upwards towards the sensor, but some of that energy will be radiated towards the ground and consequently reflected back towards the sensor. This radiance will not be perfectly reflected, as some will be absorbed by the material. However, for simplicity's sake, it is assumed that the particles absorbing this downwelled radiance are in local thermodynamic equilibrium [12].

Including the effects of a plume in scene can be done in a few short steps. The paths that govern this model are slightly more complicated than before. The atmospheric upwelling radiance remains a significant contributor to the signal, but the downwelling radiance that is reflected to the sensor now passes through the plume. The plume has a similar effect on the background thermal radiance. The resultant effect on these signals (reflected downwelling and background thermal radiance) is further attenuation based on the transmission of the plume (τ_p). The radiance of the plume material itself also contributes to the signal model. This radiance (L_p) occurs at the temperature of the plume material, and must pass through (and thus be attenuated by) the intervening atmosphere to reach the sensor. The atmospheric attenuation is assumed to be applied to the plume at the same strength it is applied to the background thermal radiance path. This is because the plume is assumed to be close to the ground, rather than much closer to the sensor. The result of these effects can be written as

$$L_{plume}(\lambda) = L_u(\lambda) + L_g(\lambda)\tau_{atm}(\lambda)\tau_p(\lambda) + L_p(\lambda)\tau_{atm}(\lambda) + L_p(\lambda) \quad (14)$$

This statement describes many of the important paths and their terms, but what is desired is to express this model with a signal term (and an associated strength) and an additive noise term. The signal term should also be a function of the signature of the chemical being detected, $b(\lambda)$. The linear expression from this model that explicitly involves $b(\lambda)$. The transmission of the plume can be expressed as follows:

$$\tau_p(\lambda) = \exp(-c b(\lambda)) \approx 1 - c b(\lambda), \quad (15)$$

where c is the column density of the gas plume, and the chemical signature of the gas is $b(\lambda)$. This transmissivity is approximately linearized using the assumption that $cb(\lambda)$ is small. The assumption of a small $cb(\lambda)$ must be kept true, otherwise the linear model will be unfaithful to the physical process.

A linear model with an additive noise term can now be realized using the result in (14). By allowing the background, or noise term to be:

$$n(\lambda) = L_u(\lambda) + [B(\lambda, T_g)\varepsilon_g(\lambda) + L_d(\lambda)(1 - \varepsilon_g(\lambda))] \tau_{atm}(\lambda) \tau_p(\lambda) + L_n(\lambda) \quad (16)$$

and letting the signal term be $b(\lambda)$ and its associated strength term be

$$e(\lambda) = c [B(\lambda, T_p) - B(\lambda, T_g)\varepsilon_g(\lambda) + L_d(\lambda)(1 - \varepsilon_g(\lambda))] \tau_{atm}(\lambda) \tau_p(\lambda) \quad (17)$$

the model can be expressed linearly as

$$L_{plume}(\lambda) = e(\lambda)b(\lambda) + n(\lambda) \quad (18)$$

This can then be expressed in vector notation by letting each entry indexed by i in the vectors correspond to a λ_i that is significant because of a sensor being used or some other practical motivation. Then let:

$$L_{plume} = L_u + [B(T_g) \otimes \varepsilon_g + L_d(1 - \varepsilon_g)] \otimes \tau_{atm} + L_n + \dots \quad (19)$$

$$\dots \dots \dots c b \otimes [B(T_p) - (B(T_g) \otimes \varepsilon_g + L_d(1 - \varepsilon_g))] \otimes \tau_{atm}$$

and let the linearization assignments be made for these terms in the same way they were made for the wavelength-continuous expressions. These values can now be assigned to the vector-valued variables in (5):

$$z_i = L_u + [B(T_g) \otimes \varepsilon_g + L_d(1 - \varepsilon_g)] \otimes \tau_{atm} + L_n \quad (20)$$

and in this case, the signal strength term is actually expressed as an element-by-element multiply where $e \otimes b$ results in the signal strength being applied. The value of this strength term is

$$e = c [B(T_p) - (B(T_g) \otimes \varepsilon_g + L_d(1 - \varepsilon_g))] \otimes \tau_{atm} \quad (21)$$

For the purposes of this work, however, the element-by-element scaling is assumed to have been applied to the known spectrum b as a pre-processing step, so only the column density c remains as a signal strength scaling term e (26). The linear model (15) reiterated at the beginning of this section can now be constructed using these assignments. This allows the processing techniques based on these linear models to be applied with great success. This development shows that the linear model is a valuable, and effective approximation to the radiometric models. It is also clear that when assumptions about column density being small or the plume being close to the ground are broken, this model may cause algorithm performance to degrade.

The detection and identification of a chemical agent is performed through post-processing of the recorded hyperspectral. Measurement of the background is performed to obtain the covariance matrix of the scene. This covariance is used to calculate the clutter-matched filters for several gas signatures from a library based on PNNL data. On each scene measurement, the background is removed and the calculation of the image of clutter-matched filter scores is performed. To detect and identify a given chemical agent, the score from calculations CMF must exceed a given threshold [7, 12, 13].

The measurements on a laboratory test stand were performed in order to determine the minimal gas concentration which can be detected by the HyperCam LWIR spectroradiometer using the method detection and identification described above. The flow from gas cylinder was controlled by a precise gas pressure regulator and a large-area blackbody was used to determine the value of thermal contrast between the gas cloud and the background. The applied blackbody has a radiative area of 11 x 11 inch and its temperature difference ΔT can be set with respect to the ambient or temperature value measured by an external sensor. In our case this external sensor was placed at the output of a gas nozzle thus the thermal contrast between the gas cloud and the background (blackbody area) could be precisely set.

4. Software for detection and identification of chemical agents

The following gases were used during the measurements: NO₂, CO₂ and propane-butane mixture, all of those having absorption lines in the far infrared spectral range. The applied gas pressure regulator provided the controlled gas flow. During the measurement session the flow was set at 5 mg/s which corresponded to gas concentration of 1% in the measurement zone observed by a HyperCam LWIR. Spectral characteristics of gases were measured for the following values of thermal contrast: $\Delta T = 1$ K, $\Delta T = 2$ K, $\Delta T = 3$ K. In order to obtain the best possible accuracy, the spectral resolution was set at 0.75 cm⁻¹, whereas the frame rate was 0.3 Hz and it resulted from the chosen resolution of sub-frame windowing (limited area of an array used during measurements which also reduced the field of view). Each measurement was repeated twice in order to avoid accidental errors. The results obtained from the HyperCam LWIR spectroradiometer gave finally the spectral characteristics of selected gases for different measurement conditions. The experimental results showing the measured spectral characteristics of CO₂ and NO₂ for different thermal contrast are presented in prior references [6, 7].

Verification of the correct operation of the algorithm was conducted by detecting and measuring the vapors of selected chemical compounds, such as 1-propanol and methanol. Those substances in liquid state were poured into a flat vessel and a gas cloud was emitted due to evaporation. Thermal contrast was modified by changing the temperature of a blackbody located in the background behind the vessel. The concentration results given by the tested algorithm were compared with the calculated ones derived from analytic description of the evaporation process. The results obtained during laboratory tests are presented in Fig. 2. This figure shows the images (calculated from datacube) recorded at wavenumber $k = 970$ cm⁻¹ and $k = 1155$ cm⁻¹ outside the methanol absorption band, and the image recorded at $k = 1085$ cm⁻¹ inside the methanol absorption band (methanol vapor clearly visible on images extracted from datacube).

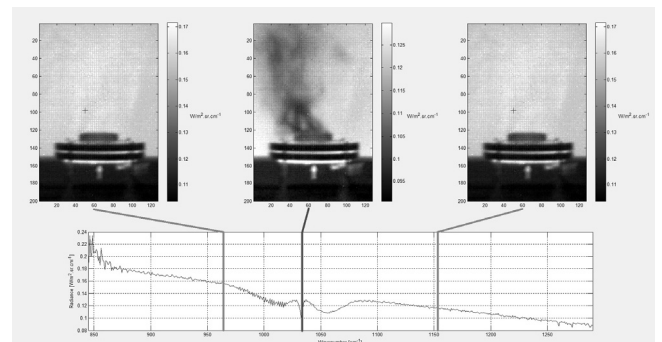


Fig. 2. The images recorded by the IFTS HyperCam during laboratory tests
Rys. 2. Obrazy zarejestrowane za pomocą obrazowego fourierowskiego spektrometri HyperCam podczas badań laboratoryjnych

The spectral characteristics obtained after post-processing analysis of the measurement data for a specified measurement point (indicated as a red cross) are presented in Fig. 2 below the image of the registered scene. The results correspond to the measurements of the methanol evaporation depicted on images.

The method of gas detection and identification (based on CMF and SAM) utilizing hyperspectral data recorded by HyperCam LWIR was implemented in a new software Reveal DRI (Fig. 3). This software package is capable of determining experimental conditions, recording measurement data and automatic gas detection and recognition using internal database of spectral data of chemical compounds.

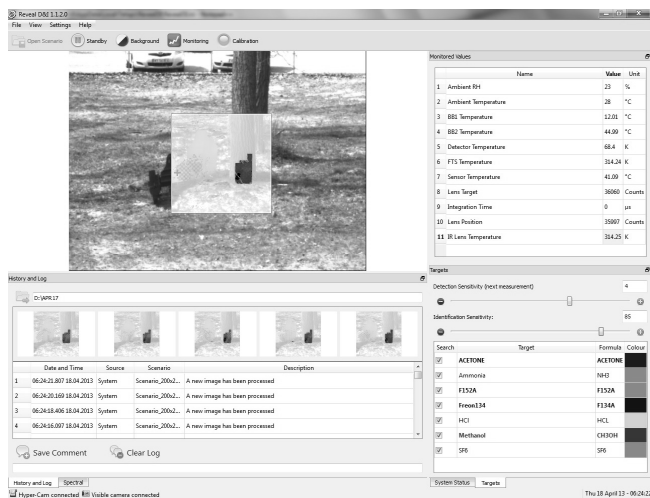


Fig. 3. The new software Reveal DRI

Rys. 3. Okno nowego oprogramowania Reveal DRI

The software takes full control over a spectrometer and its measurement settings and is capable of real-time data recording and displaying the image of the observed scenery.

The processing speed of the software is determined mainly by the spectral resolution of the data recorded by a spectrometer (the higher the resolution is, the longer it takes to process it and visualize the results on the screen). The chosen spectral resolution depends also on the spectral properties of the detected compounds - narrow absorption bands require higher spectral resolution settings during measurements. An operator can also manually adjust detection and identification thresholds, which affects the false alarm rate and probability of correct detection.

The new software was tested in field conditions in order to verify its correct operation. The following set of chemical compounds was used to test gas detection capability: vapors of 1-propanol and methanol. The results of detection and identification of methanol vapors prove that the gas detection method implemented in Reveal DRI is valid and the software operates correctly (Fig. 4).



Fig. 4. The image recorded by IFTS HyperCam during field tests

Rys. 4. Obraz zarejestrowany za pomocą obrazowego fourierowskiego spektrometru HyperCam podczas badań poligonowych

At a distance of 30 m from IFTS HyperCam there were two vessels with methanol and 1-propanol, which as a result of vaporization coupled both compounds. During the experiment in the software there were selected seven different compounds, which were irrelevant as possible to detect using the algorithms implemented in reveal DRI. The results are shown in Fig. 4 (on right images we can find the detected methanol whose clouds are red).

5. Conclusion

IFTS is a very useful method for gas detection in the open space. The possibility to present the results in a form of an image is a clear advantage, because the gas can be not only detected, but also located in space. On the basis of the conducted experiments it can be stated that the gas concentrations exceeding 1% can be detected in the open space using the HyperCam spectrometer.

The measurements previously conducted by means of IFTS spectrometers had lower accuracy due to lower sensitivity, the influence of weather conditions (mainly wind speed) and unknown thickness of a visualized gas cloud. This new method combining mathematical analysis, data from reference signature database (PNNL database), CMF (Clutter Matched Filter) module should improve the effectiveness of gas detection by IFTS-based solutions. The new algorithm implemented into new software gives the possibility of detection and identification of a very small concentration of gaseous compounds.

6. References

- [1] Harig R., Matz G.: Toxic Cloud Imaging by Infrared Spectrometry: A Scanning FTIR System for Identification and Visualization. *Field Analytical Chemistry and Technology*, 5(1-2), 75-90, (2001).
- [2] Griffin M. K., Kerekes J. P., Farrar K. E., Burke H. H. K.: Characterization of Gaseous Effluents from Modeling of LWIR Hyperspectral Measurements, *Proc. of SPIE*, 4381, 360-369, (2001).
- [3] Tremblay P., Savary S., Rolland M., Villemaire A., Chamberland M., Farley V.: Standoff gas identification and quantification from turbulent stack plumes with an imaging Fourier-transform spectrometer. *Proc. of SPIE*, 7673, 76730H, (2010).
- [4] Spisz T.S., Murphy P.K., Carter C.C., Carr A.K., Vallières A., Chamberland M.: Field test results of standoff chemical detection using the FIRST. *Proc. of SPIE*, 6554, 655408, (2007).
- [5] Farley V., Chamberland M., Lagueur P., Vallières A., Villemaire A., Giroux J.: Chemical agent detection and identification with a hyperspectral imaging infrared sensor. *Proc. of SPIE*, 6661, 66610L, (2007).
- [6] Kastek M., Piątkowski T., Trzaskawka P.: Infrared imaging Fourier transform spectrometer as the stand-off gas detection systems, *Metrology and Measurement Systems*, Vol. XVIII, No. 4, pp. 607-620, (2011).
- [7] Kastek M., Piątkowski T., Dulski R., Chamberland M., Lagueur P., Farley V.: Hyperspectral Imaging Infrared Sensor Used for Chemical Agent Detection and Identification, *Sym. on Phot. and Opto. SOPO 2012*, art. no. 6270545 (2012).
- [8] Theiler J., Foy B. R. & Frasier A. M. (2007): Beyond the adaptive matched filter: nonlinear detectors for weak signals in high-dimensional clutter. *Proc. SPIE*, vol.6565, no. 3.
- [9] Fisher R. (1936): The use of multiple measurements in taxonomic problems. *Annals of Eugenics*, vol. 7, pp. 179-188.
- [10] Czerwinski R. N., Upham C. A., Wack E. C., Burke K. & Griffin M. K. (2005): A procedure for embedding effluent plumes into LWIR imagery. *Proc. SPIE*, vol. 5806, no. 1, pp. 78-87.
- [11] O'Donnell E. M., Messinger D. W., Salvaggio C. & Schott J. (2004): Identification and detection of gaseous effluents from hyperspectral imagery using invariant algorithms. *Proc. SPIE*, vol. 5425, pp. 573-582.
- [12] Kuo S. D., Schott J. R. & Chang C. Y. (2000): Synthetic image generation of chemical plumes for hyperspectral applications. *Optical Engineering* vol. 39, no. 4, pp. 1047-1056.
- [13] Kastek M., Piątkowski T., Dulski R., Chamberland M., Lagueur P., Farley V.: Method of gas detection applied to infrared hyperspectral sensor, *Phot. Lett. of Poland*, 4 (4), 146 (2012).

otrzymano / received: 14.06.2013

przyjęto do druku / accepted: 01.08.2013

artykuł recenzowany / revised paper